J. Fluid Mech. (1974), *vol.* 63, *part* 2, *pp.* 237–255
Printed in Great Britain

Vortex pairing: the mechanism of turbulent mixing-layer growth at moderate Reynolds number

By C. D. WINANT† AND F. K. BROWAND

Division of Engineering and Applied Mechanics, University of Southern California, Los Angeles, California 90007

(Received 25 June 1973)

A mixing layer is formed by bringing two streams of water, moving at different velocities, together in a lucite-walled channel. The Reynolds number, based on the velocity difference and the thickness of the shear layer, varies from about 45, where the shear layer originates, to about 850 at a distance of 50 cm. Dye is injected between the two streams just before they are brought together, marking the vorticity-carrying fluid. Unstable waves grow, and fluid is observed to roll up into discrete two-dimensional vortical structures. These turbulent vortices interact by rolling around each other, and a single vortical structure, with approximately twice the spacing of the former vortices, is formed. This pairing process is observed to occur repeatedly, controlling the growth of the mixing layer. A simple model of the mixing layer contains, as the important elements controlling growth, the degree of non-uniformity in the vortex train and the 'lumpiness' of the vorticity field.

1. Introduction

The region between two parallel streams moving at different speeds is probably the simplest free shear flow which can be considered, since the driving velocity difference across the layer is maintained everywhere. The shear layer is usually in a turbulent state, which is to say that as a function of time the velocity at a fixed point undergoes large fluctuations of random phase in a broad frequency band. It is the random properties of the turbulent field which render the theoretical problem extremely difficult and, in spite of the numerous important contributions, there is at present no deterministic theory predicting the detailed flow field.

Existing knowledge is concentrated in two distinct areas. The first concerns the growth of small disturbances near the origin of the laminar shear layer. Comprehensive reviews of this topic have recently been given by Michalke (1970) and by Stuart (1971). On the other hand, considerable experimental evidence is available concerning fully turbulent mixing layers. There have been three recent investigations which complement one another and the classical work of Liepmann & Laufer (1947). Wygnanski & Fiedler (1970) have repeated many of the previous

† Present address: Scripps Institution of Oceanography, University of California at San Diego, La Jolla, California 92037.

statistical measurements using conditional sampling techniques to define turbulent and non-turbulent zone averages. Reynolds numbers, based upon the mean velocity difference and the mixing-layer thickness, varied between 2400 and 74000 over a downstream distance of 0·6 m. Spencer & Jones (1971) have examined the mixing layer between two streams moving at different velocities for various values of the velocity ratio. Reynolds numbers were in the range 6000–150000 over a measurement distance of 1·6 m. Brown & Roshko (1971) have investigated the effect of a density difference upon the spreading rate of a two-dimensional mixing layer. Their apparatus was pressurized to obtain Reynolds numbers in the range 7000–240000 over a downstream working distance of 15 cm.

There remains a gap between the results of the work pertaining to the linear instability of shear layers and the descriptions of turbulent mixing layers reported above. The present investigation is undertaken in the hope of furnishing clues helpful to bridging this gap by following the development of a shear layer from its inception into the fully turbulent regime. Reynolds numbers based upon shear-layer thickness vary from 45 to 850 over a 50 cm downstream distance. In terms of the wavelength of the initial unstable wave, the flow field examined is roughly 70 wavelengths in extent. Flow visualization has been used, together with hot-film measurements of conventional mean properties, and statistical measurements aimed at defining ensemble-averaged properties of the structures observed in the visual studies.

2. Experimental apparatus

The flow field is generated in a continuously operating channel, see figure 1, in which two layers of fluid of different velocity are brought together. Briefly, each layer is gravity fed from a reservoir 6 ft above the level of the channel. The mass flow in each layer is controlled by a diaphragm valve and monitored with a flowmeter. Flow velocities in the test section can be varied from 1 to 15 cm/s. The flow passes through a stilling section containing stacked straws and screens, and then through a 9 : 1 contraction to the channel. The two layers are separated by a splitter plate in the stilling section and contraction. The splitter plate terminates at a fine mesh screen, which effectively removes the previous boundary-layer growth. The plate wake is thus very thin, and is in fact undetectable 1 cm downstream of the origin. Slight flow non-uniformities of the order of 5% of the local mean velocity are introduced by this screen, but disappear within a few centimetres of the origin. The free-stream turbulence level is typically 0·5% of the local mean velocity. Dye can be injected through the upper side of the splitter plate just upstream of the screen. In addition, dye can be introduced into the main streams just ahead of the screen by the use of two small tubes which extend, respectively, through the top and bottom of the channel.

The test section, 10 × 10 cm and 1·5 m long, has a free surface so that probes may be introduced into the flow field. A carriage supported on air bearings rides above the channel and can be towed along the test section at variable speed. The carriage is used for two purposes: in the flow visualization experiments a camera is mounted on the side of the platform facing the test section, and is

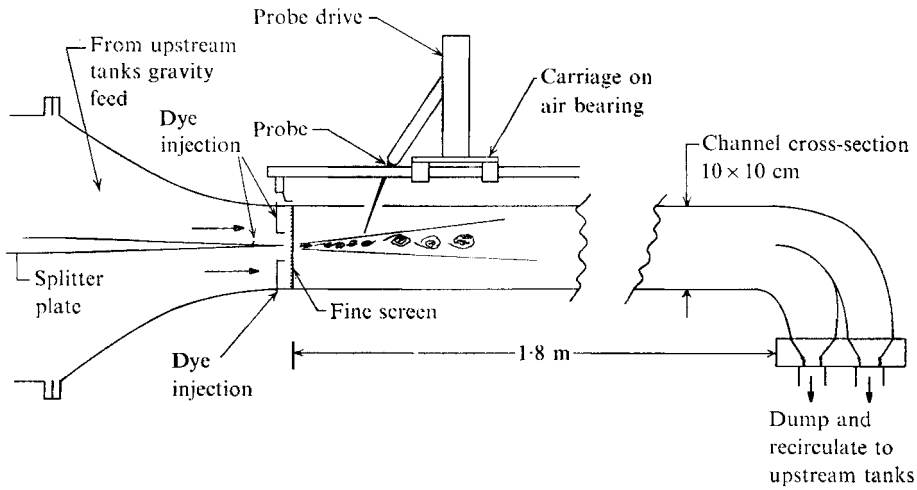

FIGURE 1. Schematic diagram of apparatus. (Not to scale.)

towed at the mean flow velocity; the carriage is also used to calibrate the hot-film probes, which are towed at known speeds through still water. The carriage supports a motor-driven probe drive with two degrees of freedom. The probe drive is programmed to move vertically (or horizontally) at a set rate and to stop at selected locations. A voltage proportional to the probe position is also provided.

For this experiment, the velocity of the upper layer is 1·44 cm/s and that of the lower layer is 4·06 cm/s: these figures correspond to a mean velocity $\overline{U}$ of 2·75 cm/s and a velocity difference ΔU of 2·62 cm/s. The Reynolds number, based on the velocity difference and the momentum thickness θ of the shear layer, varies from 8 near the origin (where θ is of the order of 0·03 cm) to 150, some 50 cm downstream.

3. Mean flow measurements

Quantitative measurements of mean velocity profiles, mixing-layer growth and the distribution of velocity fluctuations are obtained by traversing the flow field with a hot-film probe in the vertical (y) direction at fifteen unequally spaced x stations between 0·25 cm and 50 cm from the mixing-layer origin. The hot-film probe is traversed down continuously over 6 cm at a velocity of 0·0075 cm/s. Both the anemometer output and the probe position are recorded on tape for computer processing.

The data from a traverse are sampled at 50 ms intervals, resulting in 16000 samples for each traverse. After the outputs have been converted into a velocity u_i and a position y_i, the 16000 samples are sorted into 80 consecutive sets of 200 samples. For each set the average velocity and the average of the square of the velocity are found by evaluating

$$\overline{u}(y) = \frac{1}{200}\sum_{i=1}^{200} u_i, \quad \overline{u^2}(y) = \frac{1}{200}\sum_{i=1}^{200} u_i^2.$$

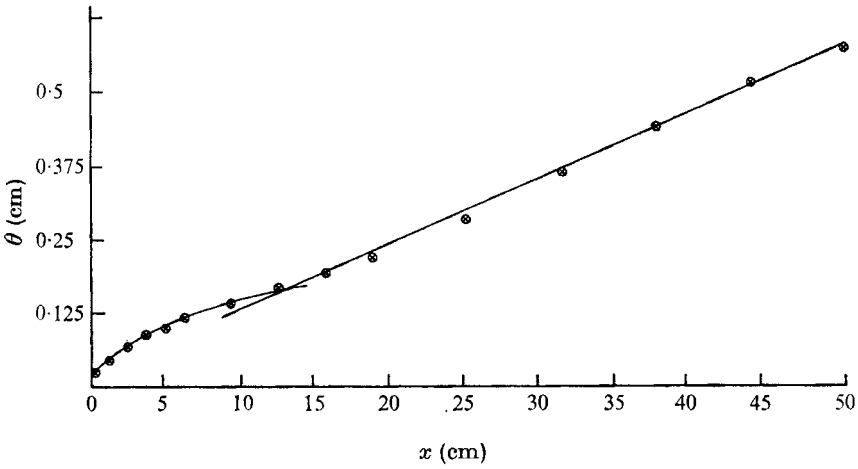

FIGURE 2. Mixing-layer momentum thickness θ as a function of downstream distance.

The root-mean-square fluctuation is then

$$u'(y) = (\overline{u^2} - \overline{u}^2)^{\frac{1}{2}},$$

while the position corresponding to each set is

$$y = \frac{1}{200} \sum_{i=1}^{200} y_i.$$

The momentum thickness θ, defined in the usual way, is

$$\theta = \int_{-\infty}^{\infty} \left[\tfrac{1}{4} - \left(\frac{\overline{u} - \overline{U}}{\Delta U}\right)^2\right] dy.$$

The growth of the momentum thickness with distance from the shear-layer origin is shown in figure 2. Distinct growth is evident in both the laminar region and the turbulent region. The laminar region in the present experiment extends some 10 cm from the shear-layer origin, and the momentum thickness grows as the square root of the downstream distance. In the turbulent region the shear layer grows linearly with the downstream distance. The measured growth rate is $d\theta/dx = 0{\cdot}011$.

Non-dimensional velocity profiles in the laminar region are presented in figure 3. The vertical position y/θ has been shifted in each case so that the abscissa variable $2(u(y) - \overline{U})/\Delta U$ is zero for all profiles at $y/\theta = 0$. Two profiles calculated by Lock (1951) for $\Delta U/\overline{U} = 2$ and $\Delta U/\overline{U} = 0{\cdot}666$ are also shown for comparison. There is very little difference between the two computations. The correlation between the present data (for which $\Delta U/\overline{U} = 0{\cdot}95$) and these profiles is excellent. Velocity profiles for the turbulent region are presented in figure 4, where the solid curve represents the experimental turbulent profile measured by Liepmann & Laufer (1947). The agreement between this curve and the results of the present experimental investigation is quite good.

Finally, some representative distributions of the root-mean-square velocity

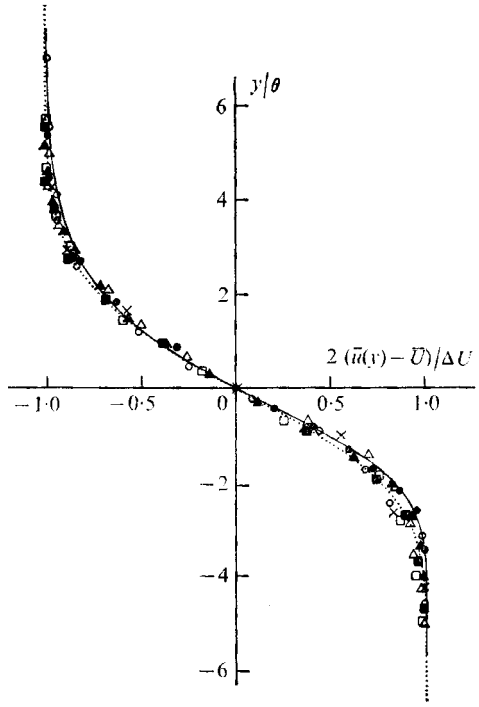

FIGURE 3. Non-dimensional mean velocity profiles in the laminar region. Distances downstream of the shear-layer origin: ×, 0·25 cm; ○, 1·25 cm; ●, 2·5 cm; △, 3·75 cm; ▲, 5·0 cm; □, 6·35 cm; ■, 9·53 cm. Theory from Lock (1951): ——, $\Delta U/\bar{U} = 2{\cdot}0$; – – – –, $\Delta U/\bar{U} = \frac{2}{3}$.

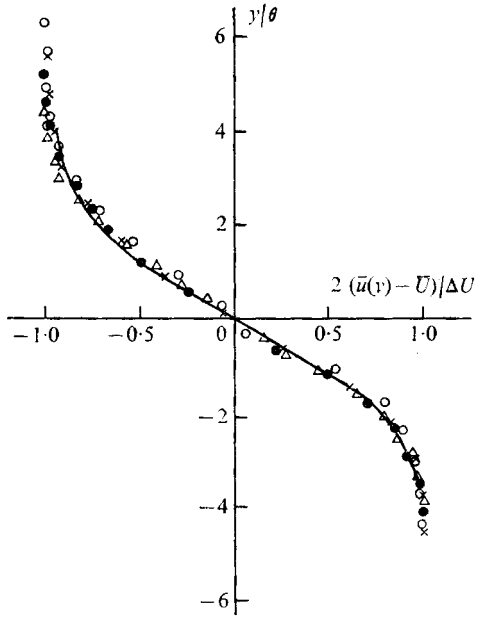

FIGURE 4. Non-dimensional mean velocity profiles in the turbulent region. Downstream distances: ×, 12·7 cm; ○, 15·9 cm; ●, 19·0 cm; △, 25·4 cm. ——, experimental, Liepmann & Laufer (1947).

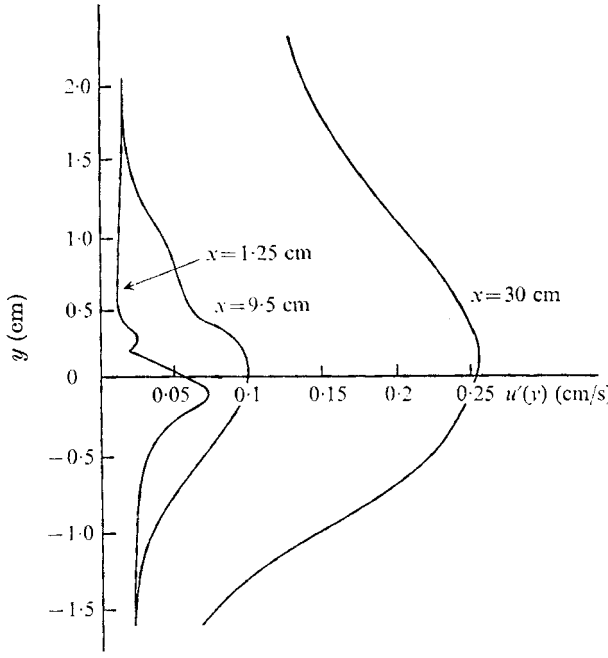

FIGURE 5. Distribution of longitudinal velocity fluctuation at three downstream locations.

fluctuation $u'(y)$ are shown in figure 5. The first distribution, measured 1·25 cm downstream of the splitter plate, resembles, qualitatively at least, the amplitude distribution of the velocity fluctuation measured by Freymuth (1966) and Browand (1966) (and predicted on theoretical grounds by Michalke 1965*b*), with a large maximum near the centre of the shear layer and a second smaller maximum on the slower moving side. The distribution measured 9·5 cm downstream of the origin shows this secondary hump to be less emphasized, while the amplitude of the larger maximum increases. The distribution measured 30 cm downstream shows a single broad maximum, and is typical of the distribution measured in fully turbulent mixing layers. The maximum disturbance amplitude is 12 % of ΔU. Liepmann & Laufer (1947) measured 17·6 %, and Spencer & Jones (1971) measured 19 %. These differences have never been explained satisfactorily, but may be due in part to Reynolds number differences.

4. The large-scale structure: flow visualization

The preceding time-averaged measurements reveal, even at these modest Reynolds numbers, a turbulent structure which is similar to the structure recorded by others. If the flow is observed visually, by introducing dye into the sheared region, a remarkably different impression of the turbulent layer emerges.

The growth of the shear layer is displayed in figure 6 (plates 1 and 2). These sequences were filmed in a moving reference frame by towing the camera carriage at the mean speed $\overline{U}$. Flow is from left to right with the lower layer having the higher velocity. The distance from the origin to the centre of each frame is shown

on the right-hand side. The shear layer itself is the heavily coloured region resulting from dye introduced on the splitter plate. The upper dye trace is from a tube placed slightly above the splitter plate.

Small waves, which characterize the linear instability region, are evident on the left-hand side of the first four photographs (the screen marking the origin of the shear layer is also visible). After two or three wavelengths, the dye marking the fluid with vorticity becomes concentrated into a periodic train of vortex structures often referred to, simply, as vortices. These large-scale structures are observed to be two-dimensional. That is, the vortical structures extend across the entire width of the channel, with no noticeable, consistent spanwise variation. The aspect ratio, defined as

$$A = \text{channel width/wavelength},$$

is here about 10–12 and is smaller further downstream.

Between 10 and 15 cm from the screen, neighbouring pairs of vortices are seen to roll around each other. Viscous diffusion smears out the identities of individual vortices to leave a single, larger vortex where originally there were two. Freymuth (1966), Browand (1966), Miksad (1972) and others have already noted this pairing and associated it with the generation of subharmonic frequencies characteristic of nonlinear growth. (Pairing has also been observed in an axisymmetric jet by Becker & Massaro (1968), and in a planar jet by Rockwell & Nicholls (1972).) None of these observers reported more than one pairing occurring,† perhaps because of the geometry of their apparatus or the short lifetime of the marker.

That the pairing process continues, however, is clearly evident from the succeeding pictures in figure 6. The history of the structure in the centre of the last photograph can be traced back and shown to be the result of four such pairings. In fact, the pairing of neighbouring vortices continues until the mixing-layer thickness has grown to the order of the channel height, at which time the top and bottom boundaries inhibit the process. (In our case, this is four pairings.) A considerable increase in smaller scale fluctuations is seen to occur at about the time of the second pairing, but the large structure remains aligned across the stream, appearing two-dimensional in the mean. The sequence presented in figure 6 is in every way typical of observations extending over tens of hours, and the conclusion is that the turbulent mixing layer grows through the combination of the large-scale vortical structures.

The relative motion of two pairing vortices may be determined by measuring the vertical and horizontal distance separating them in succeeding frames. Figure 7 shows a typical path, obtained by tracing the relative position of the vortices shown pairing in frames 7–12 of figure 6, just left of the centre. The time, in seconds, since the beginning of the pairing process, is shown on the lower side beside each position. The horizontal and vertical scales are made non-dimensional by division by the initial wavelength ($\lambda_0 = 4{\cdot}25$ cm). The diameter of the vortices in the early frame is roughly 1·1 cm while the resulting paired

† Rockwell & Nicholls (1972) note a 'triplet' formation in the developing region of a planar jet.

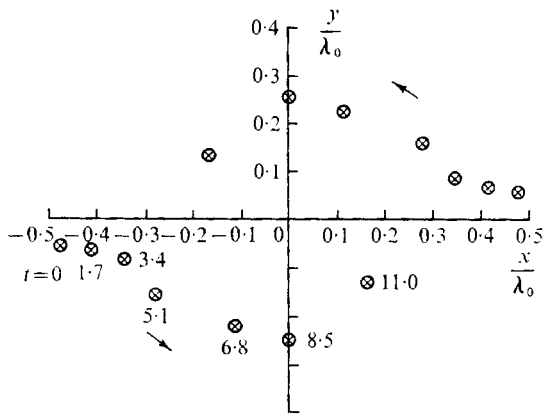

FIGURE 7. Relative positions of the centres of two pairing vortices. Time t, in seconds, is indicated. Scales are made non-dimensional by the initial spacing between the vortices.

vortex is approximately 3·4 cm in diameter. The distance travelled by the camera between frames 7–12 is 27·5 cm, so that the 'growth rate' of the shear layer, if imagined to be the change in diameter relative to the distance travelled, is 0·08. This number is very close to the growth rate of the maximum slope thickness h, given by Spencer & Jones as

$$dh/dx = 0{\cdot}081\Delta U/\bar{U},$$

where h is defined as $$h = \Delta U/(d\bar{u}/dy)_{\max}.$$

An interesting aspect of the pairing process is the deformation of the vortices. While they roll around each other, they become elongated in the flow direction, assuming a more-or-less elliptic shape with a major-to-minor axis ratio of 2. This deformation indicates that the pairing is more than a simple solid-body rotation of the vortices around each other: the induced velocities must generate strains which deform the vorticity distribution.

5. The large-scale structure: ensemble average

The flow visualization studies reported in the previous section emphasize the importance of the large-scale vortical structures in determining the growth of the mixing layer. The properties of the structures have been determined by ensemble averaging over a sufficiently large number of structures. This procedure essentially filters out the effects of small-scale turbulence and intermittency. In order to compute such an ensemble average it is necessary to define an event characteristic of the structures to be determined. Far away from the mixing-layer centre, where small-scale fluctuations are absent, potential fluctuations due to the large-scale turbulent structure can be measured. A convenient characteristic event is thus chosen to be the time at which the velocity fluctuation some distance away from the mixing-layer centre equals a given (constant) value, with a positive (or negative) slope. Two hot-film sensors are set in the same cross-flow plane. The first, the reference probe, is set at a fixed distance from the centre of the shear layer, while the second is placed at a number of different vertical

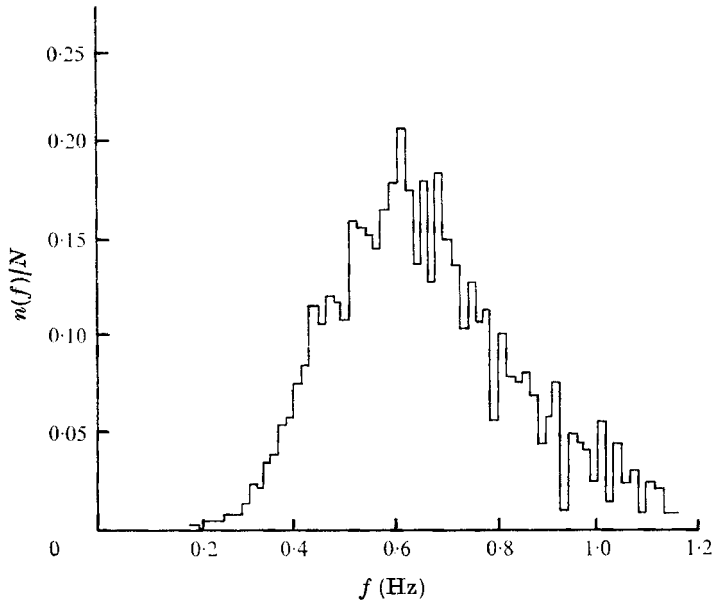

FIGURE 8. Frequencies observed by the reference probe. Total fractional portion which lies in the range $f-0{\cdot}0077 < f < f+0{\cdot}0077$ Hz.

positions across the shear layer. For each position, ensemble-average properties are then calculated by standard methods. Measurements are made in a cross-flow plane 15·25 cm downstream of the shear-layer origin. The station is in a region where turbulent growth rates are observed; it is close to the origin so that, for a given measurement time, as many structures as possible will pass by the probe: and finally, the structures observed at the station are typical of those observed elsewhere in the channel. The momentum thickness at the measurement station is 0·2 cm, and the Reynolds number based on this thickness is 52. The reference probe is placed at a position 1·5 cm above the centre of the shear layer. Velocity fluctuations are recorded by the second anemometer for 15 minute segments at thirteen y positions. The total length of time for which the signal from the reference probe was recorded was 3 hr 30 min. In this time, over 6000 fluctuation periods occurred. The histogram of the frequency of the reference signal is shown in figure 8, where $n(f)$ is the number of frequencies recorded between f_i and f_{i-1} relative to the total number of frequencies examined $N = 6000$. The mode of the histogram is $f = f_0 = 0{\cdot}6$ Hz. This corresponds to a Strouhal number $St = 2\pi\theta f_0/\overline{U}$ of 0·274. n is $1/e$ times its maximum value for

$$|f-f_0| = 0{\cdot}2 \text{ Hz}.$$

The sampled velocity fluctuations are ensemble averaged and shown in figure 9. The ordinate represents the ensemble-averaged velocity, denoted by $\langle u(y,t)\rangle$, relative to the mean velocity $\overline{u}(y)$ at that position. Curves for different y positions are offset in the vertical direction; the y position is noted on the right-hand side by the zero mark for each profile. The time scale on the abscissa is

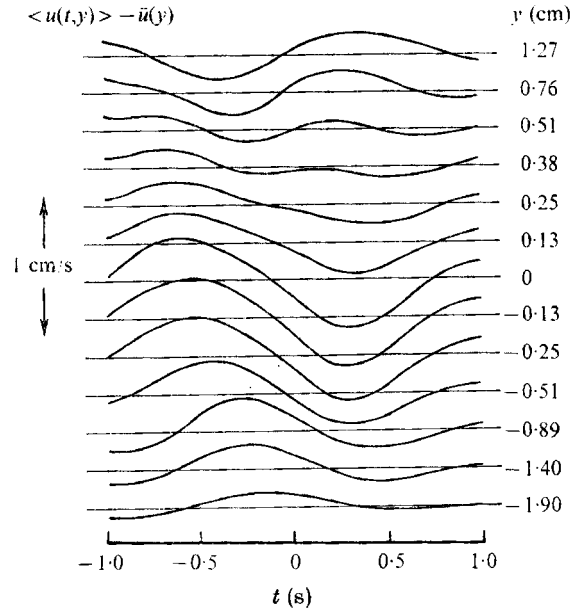

FIGURE 9. Ensemble-averaged longitudinal velocity fluctuation. The vertical position in the mixing layer is noted next to each zero-amplitude horizontal line. The horizontal scale indicates time in fractions of the total period as observed by the reference probe at the position $y = 1{\cdot}5$ cm.

referred to the moment when the velocity fluctuation sensed by the trigger probe crosses through zero with a positive slope.

The ensemble-averaged velocity variations reveal several important aspects of the flow field associated with the large-scale structures. First, this flow field is coherent across the mixing layer with a distinctly different phase on either side. The phase on the high speed side is shifted forward in time by roughly 130°. Second, the phase change across the mixing layer is a continuous one, and the amplitude of the velocity fluctuations is large near the middle of the shear layer. These facts indicate that the large-scale structure must be composed of more than a train of single vortices, since a single vortex structure would result in a sharp 180° phase change and zero amplitude along a line connecting the centres. Finally, the velocity fluctuations near the centre of the shear layer distinctly show a second hump, indicating the presence of two vortices offset in y, within the large-scale structure. This picture is consistent with the visual observations.

6. A summary of shear-layer transition

On the basis of the results of §§ 4 and 5, the following mechanism for mixing-layer growth is proposed: in the very early stages the flow field is laminar and small waves are formed, as predicted by the linear instability theory. In cases where the instability is mechanically forced, the frequency of the wave is fixed by the frequency at which the forcing mechanism is driven. In the present case,

with no forcing, the wavelength of the disturbance is that of the most unstable wave of the system (so long as the background noise shows no dominant peaks, i.e. is a reasonably 'white noise' spectrum). In either case, the result of the instability is the generation of a wavelike disturbance of some wavelength and amplitude. Naturally, when the flow is forced, the train of growing waves is more uniform than for the case of random excitation. In the region which follows the small amplitude regime, the waves are seen to grow into discrete vortices. This roll-up constitutes the earliest stage of nonlinear interaction. In the third region, which extends as far downstream as measurements can be made, the turbulent vortices are seen to interact by rolling around each other.

So far, the growth by pairing has been viewed as completely deterministic. In fact, the shear layer gradually loses knowledge of its origin, and the increased forgetfulness with increasing downstream distance is associated, for the larger scales at least, with the intermittent manner in which pairing is initiated. Pairing is a result of the instability of the row of finite amplitude vortical structures. Because pairing is promoted by small variations in the strength and spacing of the original row of vortical structures, its initiation does not always occur at the same point in space. Small spatial and temporal irregularities in the vortex structure are amplified by the progression of pairings. Also, the pairing of vortices may frequently occur in such a way as to leave an odd vortex between two pairs. These 'drop outs', which are swallowed in later pairing, increase the variations in the length scale and strengths of the vortical lumps (see figure 10, plate 3). (It is interesting to note that forcing the unstable laminar shear layer by introducing a disturbance of controlled frequency and amplitude is observed significantly to delay vortex pairing and hence, the establishment of a fully turbulent mixing layer. The reason is clear from the preceding discussion.)

When averaged over long times, the intermittency resulting from pairing is manifested as a considerable increase in the observed randomness. This is misleading, however, because one tends to miss the underlying spatial coherency by long-time averaging (e.g. compare figures 6 and 8). Spectra of the time-averaged signal at different vertical locations in the mixing layer are shown in figure 11. Most of the energy is contained in one of two frequency bands: one centred about 0·5 Hz, which corresponds to the convection of the large-scale structures downstream, and the other centred about 1 Hz, which corresponds to the disturbance generated by the interaction of individual vortices within the large-scale structure. The peaks in the spectra shift in a peculiar way towards lower frequencies on the low velocity side of the shear layer. This is more easily seen by looking along the edge of figure 11. Changes in the spectra with vertical position are attributed to Doppler shifting due to the intermittency, and serve to illustrate the complications introduced by time averaging of what is, conceptually at least, a simple process. The adjective *intermittent* might be preferred to *random*, to describe a structure which varies in time at a fixed position, but has spatial coherence over lengths comprising several of the large vortical structures at any instant.

Smaller scale disturbances are identifiable in the photographs in figure 6, and seem to appear some time after the first pairing has begun. Measurements of the

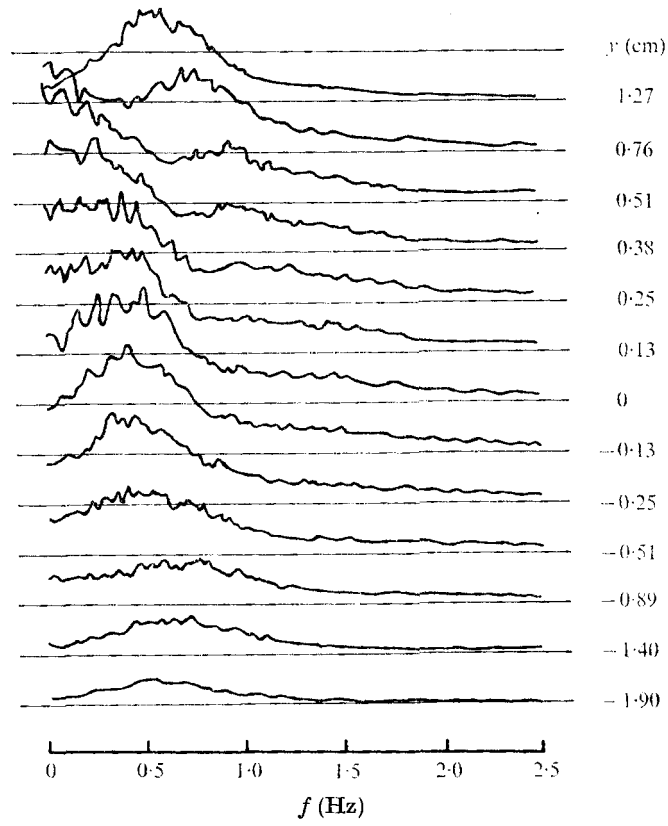

FIGURE 11. Frequency spectra of the time-averaged longitudinal fluctuation at various vertical positions in the mixing layer.

r.m.s. fluctuation amplitude, filtered to remove the low frequency components, suggest that a gradual increase in the high frequency content begins at the same place. There is some evidence to indicate that smaller scale disturbances are produced at certain phases of the pairing, but further work is required to establish this result.

One visualizes, then, large-scale turbulent vortical lumps which are continually in the process of rotating around one another in pairs. Non-turbulent fluid is absorbed or entrained, not so much by the lateral spreading of the turbulent interface, but by the engulfment of irrotational fluid trapped between the pairing structures. Figure 12(*a*) (plate 4) shows the entrapment of dyed fluid placed above and below the mixing layer. The sequence begins at a point 24 cm from the origin, where the third pairing is in progress. The centre of each succeeding frame is displaced approximately 6·4 cm downstream. It is helpful to visualize not just the fluid marked by the dye lines, but also the fluid contained between the two lines. All this fluid is in the process of being ingested by the vortical lumps. The motion induced by the localized regions of vorticity causes a periodic fattening and thinning of the fluid region contained between the dye lines. This is very similar to the original process of instability (see § 7). Fluid to be entrained is

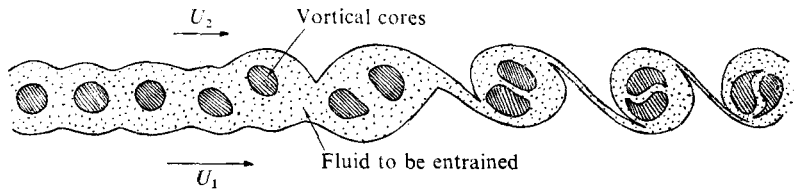

FIGURE 13. Schematic diagram of entrainment process as a function of downstream distance, or alternatively, as a function of time while riding with the mean speed.

actually transported to the opposite side of the mixing layer before being rolled up into the turbulent core. There it is trapped and homogenized by the smaller scales. There is no qualitative difference between entrainment on the high speed side (bottom) and the low speed side (top). The second sequence (figure 12(*b*), plate 5) shows entrainment near a 'drop out'. Conditions are the same as for the first sequence. The vortical lump just to the left of centre in the first frame is an odd one between two pairing structures. It is eventually swallowed by the pair to the right. A schematic diagram of the entrainment is shown in figure 13. The left-to-right sequence can be viewed as an idealized instantaneous picture of the mixing layer, or alternatively as a progression in time while riding with the mean speed.

7. A model for mixing-layer growth

The initial nonlinear region

The vortical lumps which form initially from the roll-up of the most unstable wave can be explained in a physical way by an extension of the work of Holmboe (1962), who considered the inviscid instability of a constant-vorticity layer between two parallel streams. The small amplitude wave, which grows initially, distorts the boundaries of the region containing the vorticity, see figure 14(*a*), as suggested by Holmboe; This picture can be directly extrapolated in time (Browand & Winant 1973). The perturbations in the boundaries of the constant-vorticity region are easily shown to induce vertical velocities which cause the perturbations to grow. In figure 14(*b*) the vorticity-containing region becomes periodically fatter and thinner, and in figure 14(*c*) the vortical areas are on the verge of pinching off. In figure 14(*d*), the vorticity is shown as discrete lumps. This somewhat simplistic picture is in good overall agreement with observations and with the results of calculations performed by Michalke (1965*a*) using a non-linear theory due to Stuart (1961).

The region of vortex pairing

The result of the initial nonlinear growth is a row of vortical structures containing most of the vorticity originally distributed in the steady shear layer. It would be difficult to reconcile this picture with the notion of finite amplitude waves. These structures are not waves, although hot-wire traces may show the unsteady velocity to be roughly sinusoidal and roughly periodic. It is precisely the

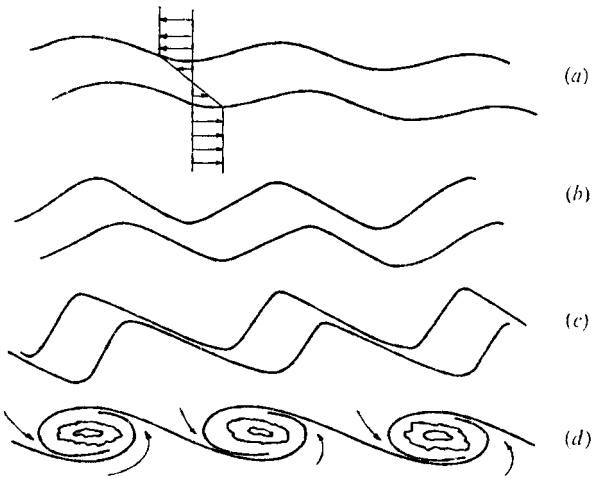

FIGURE 14. Schematic diagram of the initial instability of the shear layer, and the roll-up into discrete vortices.

departures from periodicity which are important. The pairing process results from the mutual interaction of neighbouring vortices and this, in turn, depends upon slight imperfections in the vortex spacing and strength.

It has long been recognized (e.g., Lamb 1945, § 156) that an infinite row of point vortices of the same sign and strength is a solution to the inviscid equations which is unstable to small disturbances. Stuart (1967) has found a solution having distributed vorticity which describes an infinite row of vortices with spacing λ and circulation Γ. The stream function $\psi(x,y)$ and the vorticity distribution $\Omega(x,y)$ are given by

$$\psi(x,y) = \frac{\Gamma}{4\pi} \ln\left(\cosh\frac{2\pi y}{\lambda} - \alpha\cos\frac{2\pi x}{\lambda}\right), \tag{7.1}$$

$$\Omega(x,y) = \frac{\Gamma(1-\alpha^2)}{[\cosh(2\pi y/\lambda) - \alpha\cos(2\pi x/\lambda)]^2}. \tag{7.2}$$

The parameter α indicates how concentrated the vorticity is. $\alpha = 0$ corresponds to uniform vorticity on lines of constant y, while $\alpha = 1$ corresponds to the solution for a row of point vortices (Lamb 1945, § 156).

A model of turbulent shear-layer growth based on vortex pairing has been developed by Winant (1972). The mixing layer is considered to be a double row of Stuart vortices swept downstream at the mean velocity $\overline{U}$. The rows are vertically offset by $\epsilon\lambda$, where λ represents the horizontal distance between vortices in either row (see figure 15) and ϵ is a small parameter. The circulation around each vortex is

$$\Gamma = \tfrac{1}{2}\Delta U\lambda. \tag{7.3}$$

Calculations show that adjoining pairs of vortices, one from each row, do rotate around one another and draw closer. A measure of the corresponding growth rate γ of the mixing layer is defined to be the increased distance between

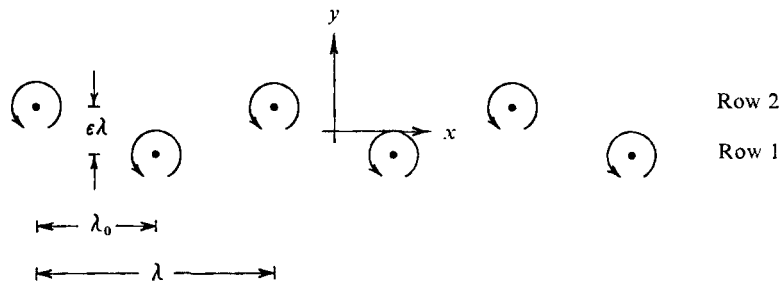

FIGURE 15. Geometry for model of vortex pairing.

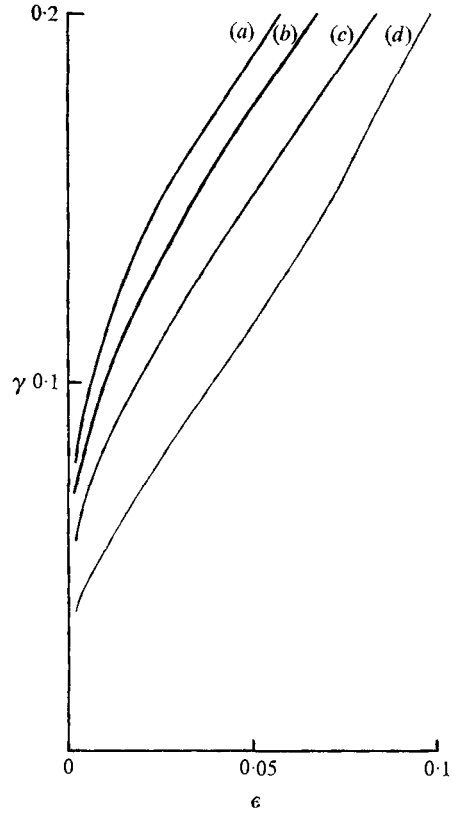

FIGURE 16. Mixing-layer spreading rate *vs.* initial perturbation in vortex spacing for various values of the vorticity concentration. (*a*) $\alpha = 1{\cdot}0$, (*b*) $\alpha = 0{\cdot}75$, (*c*) $\alpha = 0{\cdot}5$, (*d*) $\alpha = 0{\cdot}25$.

the vortex rows divided by the downstream distance travelled (at the mean velocity $\bar{U}$) in the time required to rotate the vortices through 90°. Then,

$$\gamma = (\Delta U/\bar{U}) f(\epsilon, \alpha), \tag{7.4}$$

where $f(\epsilon, \alpha)$ is a function of ϵ and α only. The predicted growth rate does not depend upon the original vortex spacing. Equation (7.4) is of the same form as

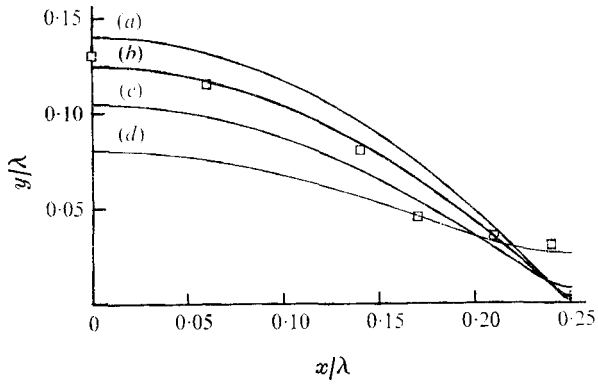

FIGURE 17. Path of vortex centre during the process of pairing. Curves: (*a*) $\alpha = 1{\cdot}0$, (*b*) $\alpha = 0{\cdot}75$, (*c*) $\alpha = 0{\cdot}5$, (*d*) $\alpha = 0{\cdot}25$. Symbols represent data taken from figure 7.

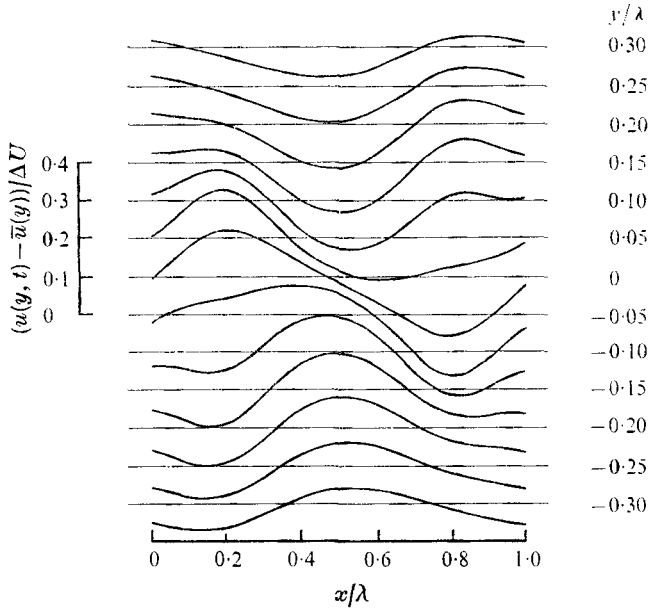

FIGURE 18. Longitudinal velocity fluctuation calculated from the vortex pairing model with $\alpha = 0{\cdot}5$. The calculation corresponds to the two rows of vortices separated vertically by $0{\cdot}072\lambda$ and horizontally by $0{\cdot}396\lambda$, giving a total phase change across the layer of approximately 130°.

the relation proposed by Spencer & Jones for the growth of the maximum slope thickness.

Figure 16 shows calculated values of γ as a function of the initial ϵ for several values of α. Clearly, the larger ϵ (corresponding in a sense to a more irregular initial distribution of vortices) the faster the growth of the shear layer, while larger values of α (corresponding to more concentrated vorticity distributions) also lead to larger shear-layer growth rates. Paths described by a pairing vortex with respect to a co-ordinate system moving with the mean velocity are shown

in figure 17, for a different value of the parameter α. In each case the value of ϵ chosen for the calculation corresponds to a γ of 0·08, which is, roughly, the measured value. Paths calculated for several other values of ϵ did not vary markedly from those shown. Measured positions of vortices during pairing are also shown (these values are taken from figure 7) and there is reasonable agreement between measured and calculated paths, the best correlation being obtained for $\alpha = 0{\cdot}5$. Finally, velocity fluctuations as a function of x/λ have been calculated for $\alpha = 0{\cdot}5$ and for a total phase shift of approximately 130° across the mixing layer. Results are shown in figure 18 for a number of vertical locations.

These calculated fluctuations are comparable, at least qualitatively, with the experimentally determined large-scale fluctuations shown in figure 9. Although the measured amplitudes are smaller, the gradual phase change across the shear layer, the finite fluctuation amplitude at the centre and the appearance of the double hump are noticeable in both figures.

8. Concluding remarks

The most important conclusion of the present investigation is that the turbulent mixing layer, at moderate Reynolds numbers, consists of large-scale vortical structures with axes perpendicular to the direction of the mean flow. Although the details of the energetics remain to be studied, it seems clear that these structures derive energy directly from the velocity difference between the two streams. In simplest terms one might think of the vortical lumps being rolled along by the difference in velocity across the mixing layer. The turbulent mixing layer grows by a repetition of the process termed 'vortex pairing', whereby two adjoining vortices interact to form a single, larger vortex.

We are inclined to think that the large-scale motions in the turbulent mixing layer will behave in a similar way at higher Reynolds numbers. It must be noted, however, that the presence of finer scales of motion will increase the diffusivity of vorticity, and in that sense, could compete with the large-scale motion tending to maintain the lumpiness of the vorticity field. Further experimental work is needed to resolve this point. The most convincing available evidence of the form of the large-scale structure at higher Reynolds numbers is found in the visual observations of Brown & Roshko (1971). Here also the 'big eddies', observed with schlieren apparatus, lie across the stream and have vorticity in the direction of the mean vorticity. Much fine-scale structure is present and the means of visualization is different, but the overall resemblence of the flow field to the vortex structure produced at lower Reynolds numbers is striking.

Both Wygnanski & Fiedler (1970) and Spencer & Jones (1971) have noted peaks in the one-dimensional energy spectra. In our case, the (lowest) peak in the spectrum of the longitudinal velocity fluctuation is associated with the passage of the paired vortical lumps. Figure 19 gives values of the non-dimensional frequency of the spectral peak in the longitudinal velocity fluctuation for the three experiments as a function of the local Reynolds number based upon mixing-layer thickness. A value of about 1·2 is obtained for the Strouhal number, independent of Reynolds number. Wygnanski & Fiedler have also presented

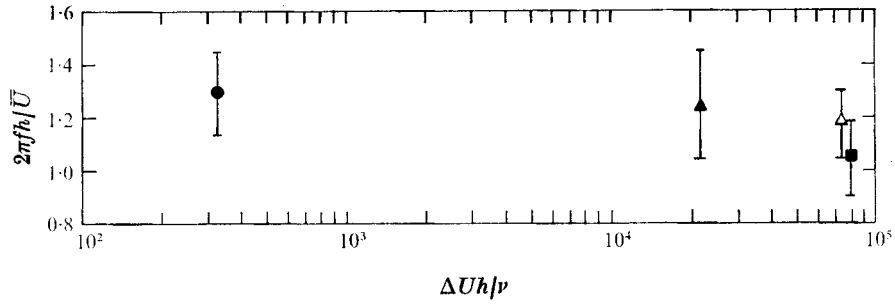

FIGURE 19. Strouhal number corresponding to the peak in the longitudinal velocity fluctuation for various experiments as a function of Reynolds number. ●, present experiments, $\Delta U/\bar{U} = 0{\cdot}95$; ▲, Spencer & Jones, $\Delta U/\bar{U} = 0{\cdot}5$; △, Spencer & Jones, $\Delta U/\bar{U} = 1{\cdot}08$; ■, Wygnanski & Fiedler, $\Delta U/\bar{U} = 2{\cdot}0$. Bars indicate approximate confidence limits.

point-averaged velocity measurements, conditioned on the passage of the turbulent interface, which indicate that the large turbulent structures are, roughly speaking, in rigid-body rotation. These results suggest structure similar to that observed in the present investigation.

It is suggested here that the vortex structures discussed above, and vortex pairing, are fundamental to the turbulent mixing layer. Vortex pairing may be important in another context. Recently there has been an effort to relate the organized structure observed in the developing region of jets to the production of acoustic noise. Crow & Champagne (1971) have noted the formation of vortex ring structures in the developing region of an axisymmetric jet at Reynolds numbers of about 80000 (based on nozzle diameter). The rings seem to come in groups which were described as 'puffs' by Crow & Champagne. Laufer, Kaplan & Chu (1973) have made indirect observations of vortex-ring pairing in an axisymmetric jet at Reynolds numbers of order 160000. They have noted the disappearance of peaks in the instantaneous pressure signals recorded just outside the developing region of the jet, and attributed this periodic loss to vortex pairing. It is, in fact, proposed that pairing of the vortex rings is the primary mechanism responsible for the production of jet noise.

The authors are indebted to Professor John Laufer, whose support and interest were a constant source of encouragement. Thanks are also due to Professor Blackwelder, Professor Kaplan and Professor Troesch of U.S.C. and Professor Kelly of U.C.L.A. for enlightening conversations. The support of the Office of Naval Research, under contract N00014-67-A-0269-0015, is gratefully acknowledged.

REFERENCES

BECKER, H. A. & MASSARO, T. A. 1968 Vortex evolution in a round jet. *J. Fluid Mech.* **31**, 435–448.

BROWAND, F. K. 1966 An experimental investigation of the instability of an incompressible separated shear layer. *J. Fluid Mech.* **26**, 281–307.

BROWAND, F. K. & WINANT, C. D. 1973 Laboratory observations of shear layer instability in stratified fluid. *Boundary Layer Meteor*, **5**, 67–77.

BROWN, G. & ROSHKO, A. 1971 The effect of density differences on the turbulent mixing layer. *Turbulent Shear Flows, AGARD Current Paper*, no. 93, §§23.1–23.12.

CROW, S. C. & CHAMPAGNE, F. H. 1971 Orderly structure in jet turbulence. *J. Fluid Mech.* **48**, 547–591.

FREYMUTH, P. 1966 On transition in a separated laminar boundary layer. *J. Fluid Mech.* **26**, 683–704.

HOLMBOE, J. 1962 The behaviour of symmetric waves in stratified shear layers. *Geophys. Publ.* **24**, 67–113.

LAMB, H. 1945 *Hydrodynamics*. Dover.

LAUFER, J., KAPLAN, R. E. & CHU, W. T. 1973 On the generation of jet noise. *AGARD Specialists Meeting 'Noise Mechanisms', Brussels.*

LIEPMANN, H. W. & LAUFER, J. 1947 Investigation of free turbulent mixing. *N.A.C.A. Tech. Note*, no. 1257.

LOCK, R. C. 1951 The velocity distribution in the laminar boundary layer between parallel streams. *Quart. J. Appl. Math.* **4**, 42–63.

MICHALKE, A. 1965*a* Vortex formation in a free boundary layer according to stability theory. *J. Fluid Mech.* **22**, 371–383.

MICHALKE, A. 1965*b* On spatially growing disturbances in an inviscid shear layer. *J. Fluid Mech.* **23**, 521–544.

MICHALKE, A. 1970 The instability of free shear layers: a survey of the state of the art. *Dsch. Luft- & Raumfahrt. Mitteilung*, no. 70–04.

MIKSAD, R. W. 1972 Experiments on the nonlinear stages of free-shear-layer transitions. *J. Fluid Mech.* **56**, 695–719.

ROCKWELL, D. O. & NICHOLLS, W. O. 1972 Natural breakdown of planar jets. *Trans. A.S.M.E., J. Basic. Eng.* **94**, 720–728.

SPENCER, B. W. & JONES, B. G. 1971 Statistical investigation of pressure and velocity fields in the turbulent two-stream mixing layer. *A.I.A.A. Paper*, no. 71–613.

STUART, J. T. 1961 On three-dimensional non-linear effects in the stability of parallel flows. *Adv. in Aero. Sci.* **3**, 121–142.

STUART, J. T. 1967 On finite amplitude oscillations in laminar mixing layers. *J. Fluid Mech.* **29**, 417–440.

STUART, J. T. 1971 Nonlinear stability theory. *Ann. Rev. Fluid Mech.* **3**, 347–370.

WINANT, C. D. 1972 Vortex pairing in a turbulent shear layer at moderate Reynolds numbers. Ph.D. thesis, Department of Aerospace Engineering, University of Southern California, Los Angeles.

WYGNANSKI, I. & FIEDLER, H. E. 1970 The two-dimensional mixing region. *J. Fluid Mech.* **41**, 327–361.

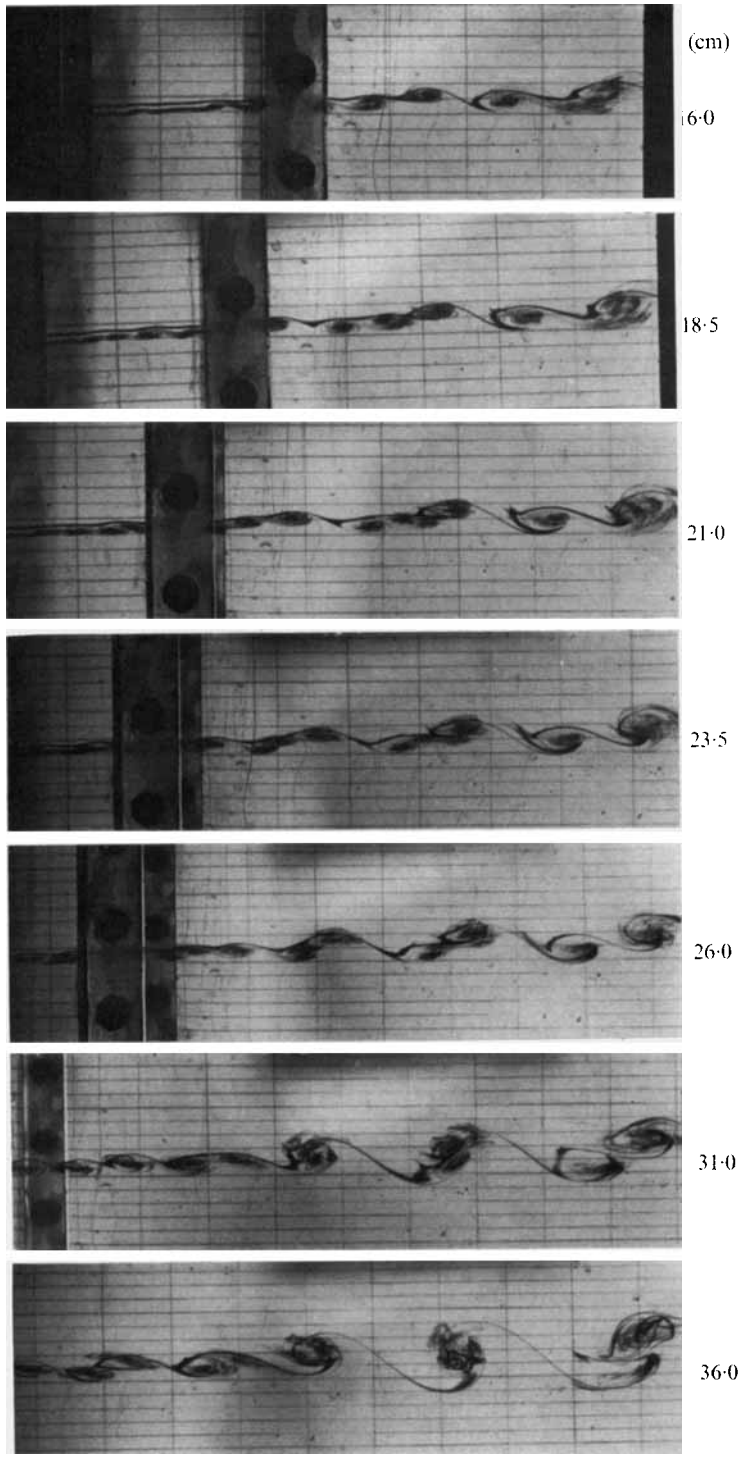

FIGURE 6(*a*). For legend see plate 2.

(*b*)

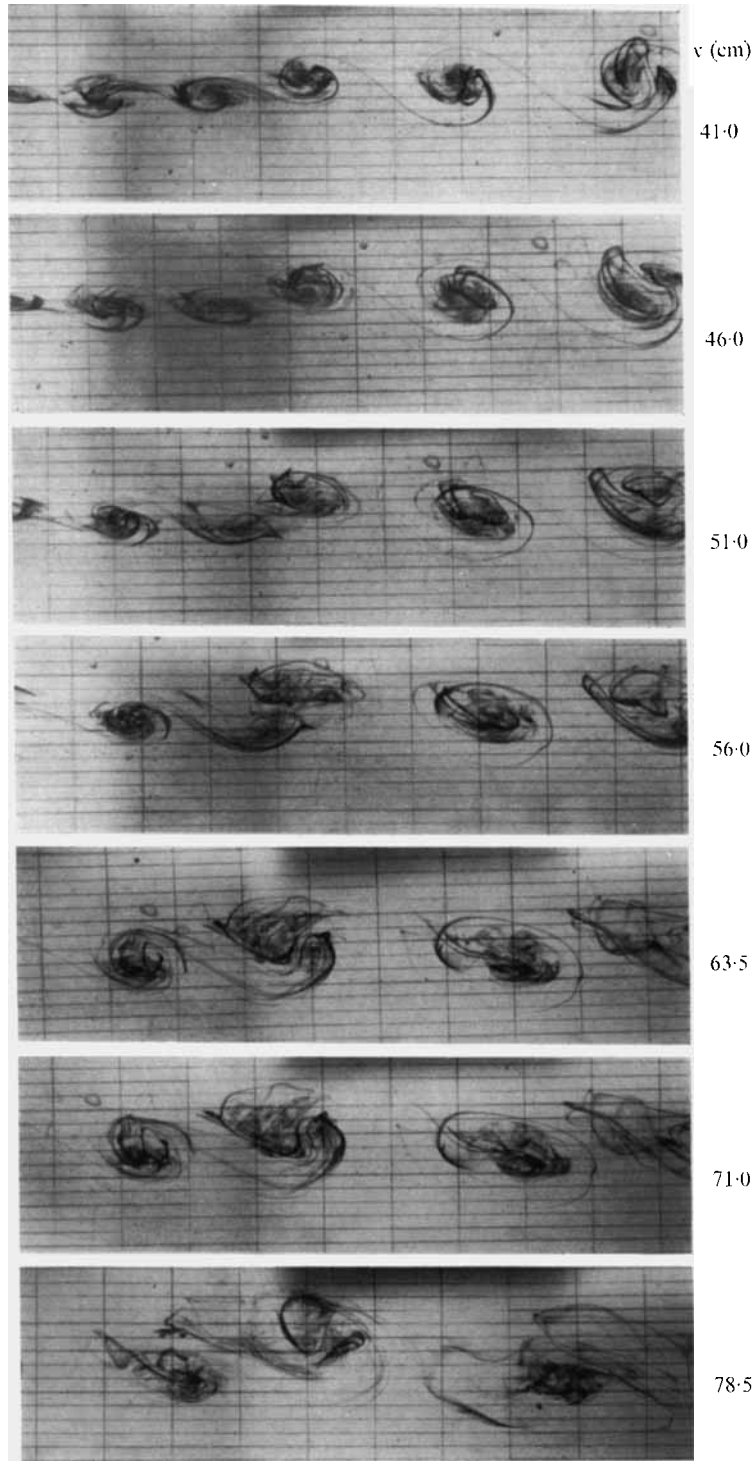

FIGURE 6. Sequence of photographs showing vortex pairing. Heavy dye line marks (the centre of) the shear layer. Upper line is dye injected just above the shear layer. Camera is moving with the mean speed $\bar{U}$. Downstream distance to the centre of each frame is indicated to the right. Background grid spacing: horizontal lines, 0·5 cm; vertical lines, 2·54 cm.

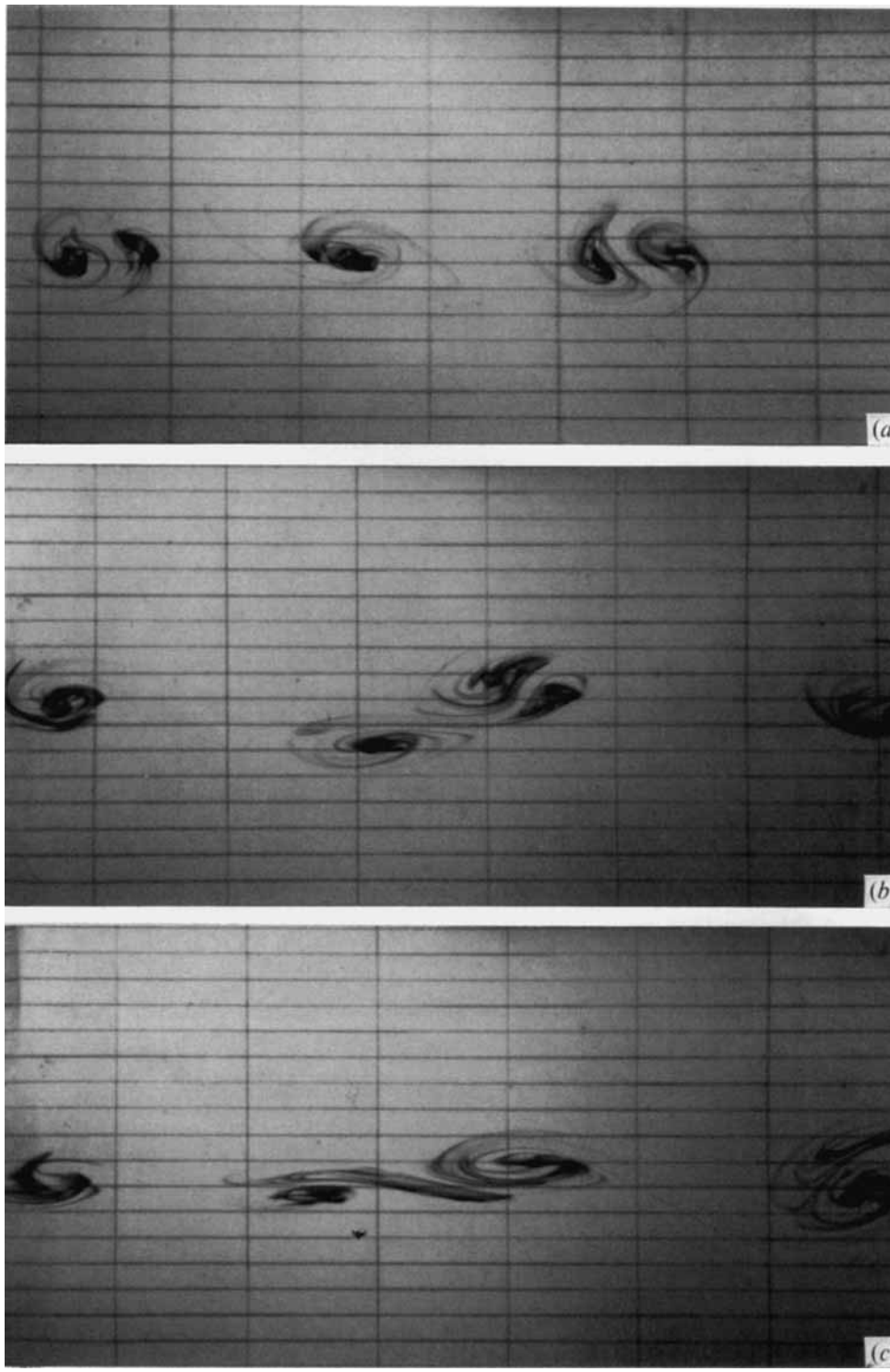

FIGURE 10. (*a*) The occurrence of an unpaired vortex between two paired structures. At later times, the unpaired vortex either (*b*) combines in a triad or (*c*) becomes stretched between two pairs. Background grid spacing: horizontal lines, 0·5 cm; vertical lines, 2·5 cm.

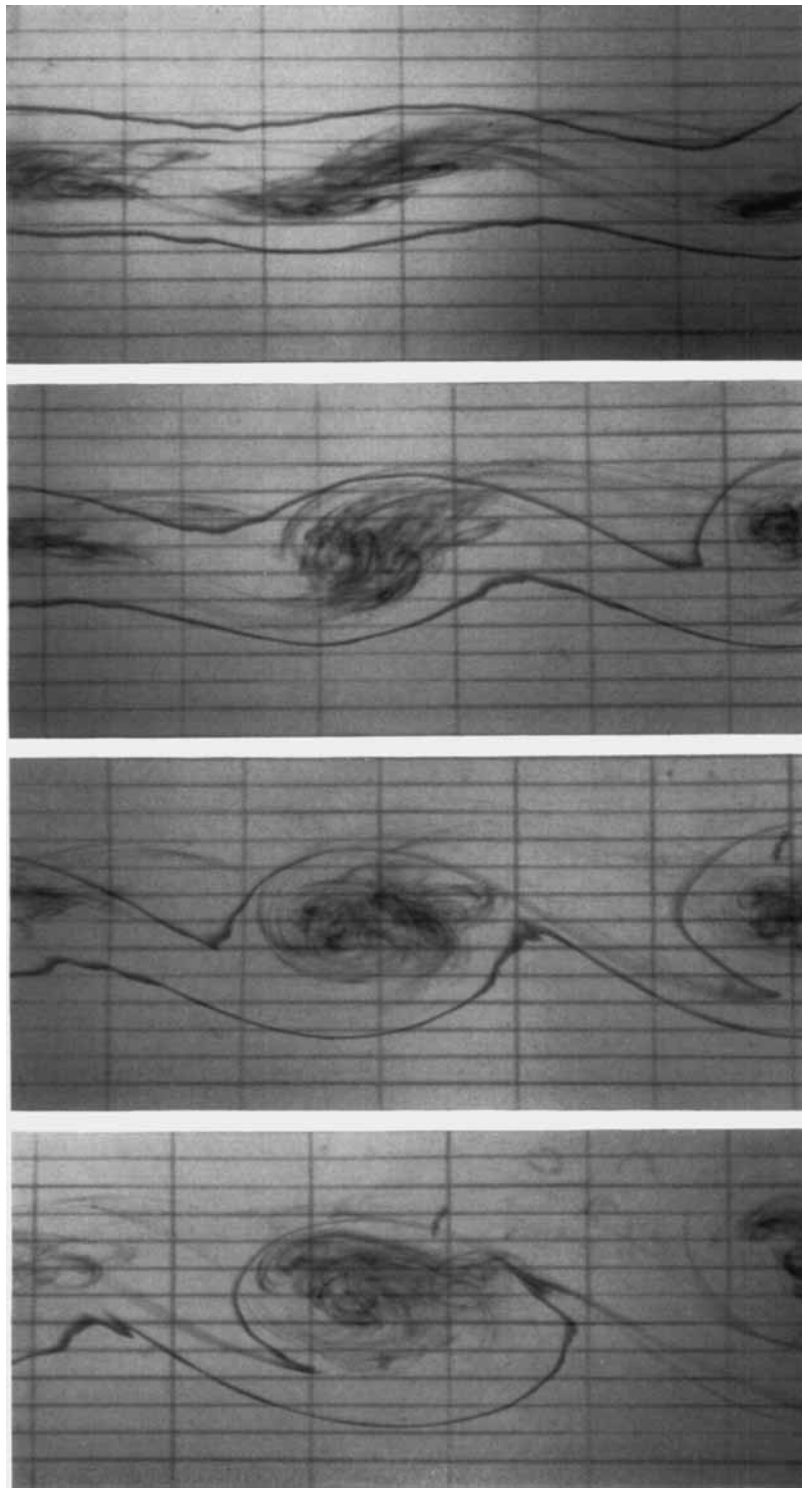

FIGURE 12(*a*). For legend see plate 5.

(*b*)

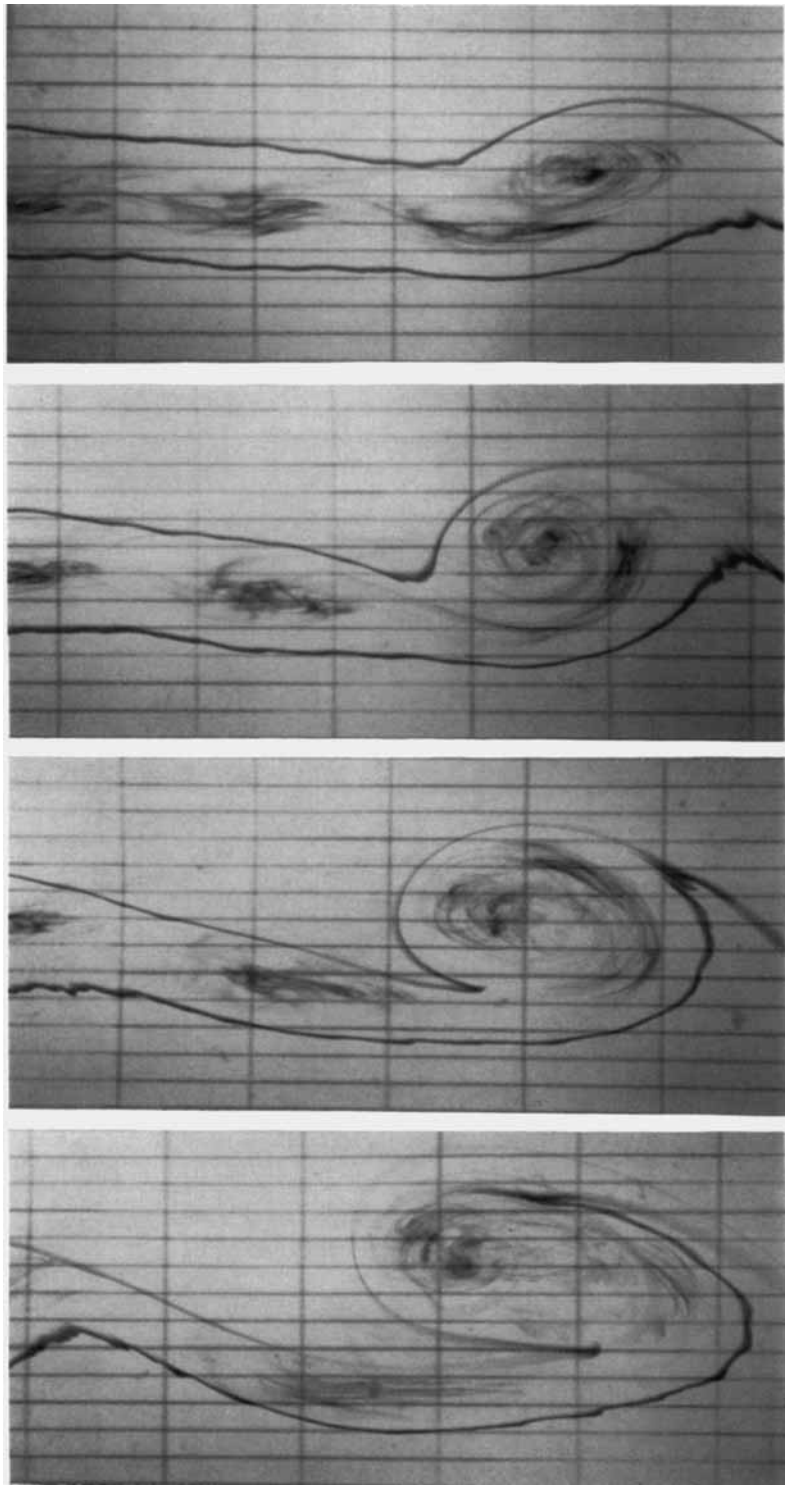

FIGURE 12. (*a*) Photographic sequence showing entrainment of the fluid between the uppermost and lowermost dye lines into the regions of high vorticity (marked by the dyed fluid in the core). (*b*) Variation of the basic entrainment process in the neighbourhood of a 'drop out'. Camera is moving at the mean speed $\overline{U}$. Centre of first frame in (*a*) and (*b*) is 24 cm downstream. Each succeeding frame is displaced 6·4 cm downstream. Background grid spacing: horizontal lines, 0·5 cm; vertical lines, 2·54 cm.